Nanostructurization effects in PVP-stabilized tetra-arsenic tetra-sulfide As_4S_4 nanocomposites

O. Shpotyuk [a, b, c], Z. Bujňáková [d], P. Baláž [d], A. Ingram [e], P. Demchenko [f], A. Kovalskiy [g], M. Vlcek [h], Ya. Shpotyuk [f, i], J. Cebulski [i], A. Dziedzic [i]

[a]*Institute of Physics of Jan Dlugosz University in Czestochowa, 13/15, Al. Armii Krajowej, Czestochowa, 42200, Poland*

[b]*Vlokh Institute of Physical Optics, 23, Dragomanov Str., Lviv, 79005, Ukraine*

[c]*Scientific Research Company "Carat", 202, Stryjska Str., 79031, Lviv, Ukraine*

[d]*Institute of Geotechnics of Slovak Academy of Sciences, 45, Watsonova Str., Ko ice, 04001, Slovakias*

[e]*Opole University of Technology, 75, Ozimska Str., Opole, 45370, Poland*

[f]*Ivan Franko National University of Lviv, 1, Universytetska Str., 79000 Lviv, Ukraine*

[g]*Department of Physics & Astronomy, Austin Peay State University, Clarksville, TN, 37044, USA*

[h]*Department of General and Inorganic Chemistry, Faculty of Chemistry, University of Pardubice, 532 10, Pardubice, Czechia*

[i]*Centre for Innovation and Transfer of Natural Sciences and Engineering Knowledge, 1, Pigonia Str., 35310, Rzeszow, Poland*

H I G H L I G H T S

- PVP-stabilized tetra-arsenic tetra-sulfide nanocomposites prepared by wet milling.
- As_4S_4-PVP composites by complementary atomic-specific and deficient structure probes.
- Surface oxidation due to crystalline arsenolite As_2O_3 under wet milling.
- Free-volume structure of PVP-stabilized As_4S_4 nanocomposites by PAL spectroscopy.
- x3-x2-coupling decomposition algorithm to treat PAL data for As_4S_4-PVP composites.

A B S T R A C T

Nanostructurization in three types of tetra-arsenic tetra-sulfide As_4S_4 polymorphs composed by (1) preferential β -As_4S_4, (2) realgar α-As_4S_4 and (3) admixture of As_4S_4 in the form of β -realgar, pararealgar and intermediate c-phase subjected to mechanochemical ball milling in a water solution of poly-vinylpyrrolidone (PVP) are characterized with multiexperimental structure-sensitive probes. Void structure of pelletized As_4S_4-PVP nanocomposites is probed by positron annihilation lifetime spectroscopy complemented with atomic-sensitive techniques such as X-ray powder diffraction, Raman scattering and scanning electron microscopy with energy-dispersive X-ray spectroscopy. Appearance of arsenolite As_2O_3 crystallites is character for all As_4S_4 polymorphs affected by wet milling. Positron annihilation lifetime data considered in terms of substitution positron-positronium trapping confirm complicated nature of nanocomposites. Modified x3-x2-coupling decomposition algorithm developed in addition to unconstrained x3-term fitting procedure is applied to parameterize annihilation channels in these nanocomposites. Interfacial free-volume voids between neighboring nanoparticles in PVP environment are defined as most favorable trapping sites, they being rather loosely composed by As_4S_4 crystallites in full respect to variety of crystallographic polymorphs used for milling. Detected annihilation channels are ascribed preferentially to intrinsic free-volume voids insensitive to trapping states at the surface of oxidized nanocomposites.

1. Introduction

Since ancient times, chemical compounds of arsenic (often also termed in medical literature as arsenicals [1,2]) have been known as promising and versatile drugs in cancer therapy owing to pronounced angiogenesis inhibition effect on a row of human malignancies [1-4]. Thus, the pronounced anticancer functionality of known tetra-arsenic tetra-sulfide As_4S_4 polymorphs has been in a sphere of tight interests in biomedicine because of promising antileukemic activity [3,4]. To overcome negative feedback due to poor bioavalibility as a consequence of limited solubility in water, these arsenicals are often used as mediated to a nanosize [5-12]. Being subjected to high-energy ball milling in solutions with some biocompatible polymers such as polyvinylpyrrolidone (PVP), they form nanostructured composites possessing excellent medicinal efficacy [10-

14]. Thus, the polymer-assembled suspensions of realgar nanoparticles (NPs) exhibit improved bioavailability and cytotoxicity as compared with coarse realgar, and, in final, enhanced pharmacological *in vitro* anticancer activity producing DNA damage and apoptosis-induced cellular effect on a number of human cancer cell lines, such as MCF7, HepG2 and A549 [5], ECV-304 [6], RPMI-LR5 and OPMI [8], H460 [10], BOWES and A375 [11], HL-60 [12], etc.

In above cases, the comprehensive information on atomic arrangement of these hybrid organic-inorganic systems plays a pivotal role to understand their anticancer behavior and prepare sulfoarsenide nanocomposites with guided anticancer functionality. Positive consequence of nanostructurization in such substances is governed not only by chemistry of NPs themselves (their structure type, respective content and phase composition), but also interconnection between different space-filling atomic fragments forming free-volume sub-structure [13-15]. To control such tiny atomic-deficient entities, the positron annihilation lifetime (PAL) spectroscopy, the probe grounded on experimental space-time continuum determination for electron interaction with its antiparticle (positron e^+) seems to be one of most promising tools [16-18]. Within this method, the electron-positron e^--e^+ interaction is employed to study atomic and sub-atomic imperfections in solids (like free-volume defects, vacancies, vacancy-like clusters and their complexes, interfacial voids and pores, intergranual boundaries, etc.) whichever their origin.

In this work, we shall analyze possibilities of PAL technique developed in combination with traditional atomic-sensitive microstructure probes such as X-ray powder diffraction (XRPD), Raman scattering and scanning electron microscopy (SEM) with energy-dispersive X-ray spectroscopy (EDS) to characterize nano-structurization effects in As_4S_4-PVP composites prepared by wet milling.

2. Experimental

2.1. Nanocomposite preparation

Nanocomposite samples were prepared using three types of coarse-grained tetra-arsenic tetra-sulfide As_4S_4 counterparts milled in laboratory circulation mill MiniCer (Netzsch, Germany) in a presence of 300 mL of 0.5% PVP solution as nonionic stabilizer. Thus, we used (1) chemical commercial arsenic(II) sulfide (95% in purity, Sigma-Aldrich, USA), (2) mineral realgar collected from Allchar locality (R. Macedonia) and (3) mineral realgar subjected to partial transformation into pararealgar owing to sunlight exposure, the corresponding sample batches being respectively marked as REA1, REA2 and REA3. The milling was performed with 5 g of arsenical under 85% loading of milling shaft with yttrium-stabilized ZrO_2 balls (0.6 mm in a diameter). More detailed description of milling procedure employed can be found elsewhere [10].

After filtration through sterile 0.22 mm filter, the separated solid phase was dried at 70 °C and pelletized under applied pressure of 0.7 GPa. This route was identical for all samples, thus the prepared pellets of PVP-stabilized As_4S_4 nanocomposites being near 6 mm in a diameter and 1 mm in a thickness. The NPs sizes in dried pellets are expected to be close to ones proper to fresh-prepared suspensions, so reaching ~100-200 nm in a diameter [10]. In a similar way, we also prepared the pelletized samples of pure PVP to use them as reference in further research.

2.2. Nanocomposite characterization

2.2.1. Atomic-specific structure characterization

The microstructure of PVP-stabilized As_4S_4 nanocomposites was studied with XRPD, the experimental data being collected in a transmission mode on STOE STADI P diffractometer with the following setup: Cu $K\alpha_1$-radiation, curved Ge (111) monochromator on primary beam, $2\theta/\omega$-scan, angular range for data collection 5.000-80.345° 2θ with increment 0.015, linear position sensitive detector with step of recording 0.480° 2θ and time per step 420-500 s, U = 40 kV, I = 37 mA, T = 24°C and relative humidity RH = 35%. Preliminary data processing and XRPD analysis were performed using STOE WinXPOW [19] and Powder Cell [20] program packages, using known information on crystal structures for the phases taken from databases [21,22]. The crystal structures of the phases were refined by the Rietveld method with the program FullProf.2k (version 5.40) [23], applying a Thompson-Cox-Hastings pseudo-Voigt profile function and isotropic approximation for atomic displacement parameters. The quantitative phase analysis according to [24] and determination of microstructural properties (average apparent crystallite size D, e.g. size of coherently diffracting domains, average maximum strain ε) were performed during the Rietveld refinement by isotropic line broadening analysis implemented in the program FullProf [25]. Intrinsic broadening was taken into consideration in the calculations, using instrumental resolution files obtained by profile fitting of the primary beam and NIST SRM 676 (Al_2O_3).

The atomic species composing As_4S_4-PVP nanocomposites were also identified with Raman scattering technique arranged at room temperature using fast Fourier-transform spectrometer IFS 55 provided with FRA 106 accessory (Bruker, Germany). The back-scattering method with Nd:YAG laser line (1064 nm) of 90 mW output power was employed for the excitation, the resolution of the spectrometer being 4 cm^{-1} at 300 scans. A more detailed description of this experimental routine can be found elsewhere [26]. The Raman scattering spectra were processed using Bruker software, normalized by standard method of matching the most intensive peaks in the studied spectral region and compared by subtraction. The Raman scattering bands were ascribed to signatures of different atomic species proper to As_4S_4-PVP system at the basis of known experimental data [26-34].

The surface morphology of the prepared As_4S_4-PVP nanocomposites was also characterized using scanning electron microscope (SEM) with EDS (energy-dispersive spectroscopy) analyzer FEI QUANTA 3D 200i (Hillsboro, OR, USA).

2.2.2. Atomic-deficient (void) structure characterization

The void structure of the As_4S_4-PVP nanocomposite pellets was studied with PAL spectroscopy. The PAL spectra were recorded with fast-fast coincidence system (ORTEC) of 230 ps resolution (the full width at half maximum of single Gaussian determined for control ^{60}Co isotope) at the temperature of 22 °C and relative humidity of 35% [18]. To ensure precise lifetime measurement, each spectrum was recorded in normal-measurement statistics reaching ~10^6 elemental annihilation events (coincidences). The channel width of 6.15 ps allows total number of channels to be 8000. The ^{22}Na isotope of low ~50 kBq activity prepared from aqueous $^{22}NaCl$ solution (wrapped by Kapton® foil of 12 mm thickness and sealed) was used as positron source sandwiched between two identical nanocomposite pellets. The best fitting of the detected PAL spectra was achieved under their decomposition into three single exponents (conventional three-term x3-decomposition route under normalized component intensities $I_1 + I_2 + I_3 = 1$), covering channels caused by positrons e^- annihilating in defect-free bulk, trapped in spatially-extended free-volume defects and forming bound positron-electron e^+-e^- state (the positronium Ps atom). This procedure was performed by processing the raw PAL spectra with LT 9.0

program [35]. The resulting accuracies in positron lifetimes τ_i and intensities I_i were not worse ±0.005 ns and 0.5%, respectively. Under such conditions, the error bar in e^- trapping rate in defects k_d does not exceed ±0.01 ns^{-1}.

The positron e^+ trapping formalism allows adequate description of PAL spectra in terms of two-state model (x2-term decomposition) with one kind of trapping defects [16-18]. The corresponding e^+ trapping modes, e.g. mean τ_{av} and defect-free bulk τ_b positron lifetimes along with trapping rate in defects k_d are defined as [16]:

$$\tau_{av.} = \frac{\tau_1 I_1 + \tau_2 I_2}{I_1 + I_2}, \quad (1)$$

$$\tau_b = \frac{I_1 + I_2}{\frac{I_1}{\tau_1} + \frac{I_2}{\tau_2}}, \quad (2)$$

$$\kappa_d = \frac{I_2}{I_1}\left(\frac{1}{\tau_b} - \frac{1}{\tau_2}\right). \quad (3)$$

In addition, the difference between defect-related and bulk positron lifetimes ($\tau_2 - \tau_b$) are calculated within x2-model as a signature of size of free-volume e^+-trapping defects in terms of equivalent number of vacancies, whereas τ_2/τ_b ratio is ascribed to the nature of these defects [16].

The positronium Ps trapping formalism concerns positrons annihilating in porous substances as free particles or pick-up an electron from environment by forming bound positron-electron e^+ - e^- state [16,17]. In the ground state, this Ps atom exists as singlet para-positronium p-Ps decaying intrinsically with two γ-quanta and character lifetime in a vacuum of 0.125 ns, and triplet ortho-positronium o-Ps decaying with three g-quanta and lifetime of 142 ns. In matter, since the positron wave function overlapping with electrons outside, the annihilation with such electrons having an antiparallel spin decreases lifetime to 0.5-10 ns resulting in two γ -rays ("pick-off" annihilation) [17]. Two conditions should be satisfied to stabilize Ps, the first being sufficiently high size of free-volume voids captured Ps and second being low electron density preventing direct e^+ - e^- annihilation (that is why metals and semiconductors are excluded as potential Ps-forming media) [16,17].

The Ps localized in free-volume spaces gives indication on their mean radii R in terms of longest τ_3 lifetimes in respect to known semi-empirical Tao-Eldrup equation:

$$\tau_3 = 0.5 \cdot \left[1 - \frac{R}{R + \Delta R} + \frac{1}{2\pi} \cdot \sin\left(\frac{2\pi R}{R + \Delta R}\right)\right]^{-1}, \quad (4)$$

where ΔR = 0.166 nm is fitted empirical electron layer thickness [17].

The relative intensity of this component I_3 correlates well with density of Ps trapping sites, giving fractional free volume f_v (in %) as

$$f_v = \mathbf{C} \cdot V_f \cdot I_3, \quad (5)$$

where V_f (in $Å^3$) is void volume in spherical approximation ($4/3\pi R^3$) and C is empirically determined constant (0.0018 for epoxy and 0.0014 for polystyrene polymers [17]).

Thus, in case of highly inhomogeneous molecular substances such as polymers or composites, the annihilation is expected through **mixed e^+-Ps trapping channels** [36-38]. These channels are mutually interconnected in nanostructurized composites so that interplay between them results in significant complication in meaningful interpretation of the detected PAL spectra. The formalism of simply separated e^+ and Ps trapping events cannot be further explored as a realistic signature of annihilation phenomenon because of uncompensated admixture in the first component arising from p-Ps [37,38]. In such a case, additional supposition on eventual behavior of mixed e^+-Ps trapping channels is needed to distinguish their contributions unambiguously and, thereby, to develop meaningful methodological algorithm of their description in dependence on structure evolution processes. In the model [36], the nanostructurization caused by incorporation of guest NPs in host matrix was described as substitution e^+-Ps trapping, e.g. process, which occurs as conversion of o-Ps traps in pure host matrix into e^+ trapping sites in NP-modified *host-quest* matrix. By accepting tight interconnection between these traps, this approach has been defined as *x3-x2-coupling decomposition algorithm*, to distinguish it from *conventional x3-decomposition* procedure dealing with PAL spectra originated from unresolved e^+-Ps trapping.
Hence, in respect to this approach [36], an additive two-state e^+ trapping model, describing conversion from Ps to e^+ trapping sites in *host* matrix due to embedded *guest* NPs, can be validated by mathematical treatment procedure allowing consideration of the measured x3-term PAL spectra in generalized x2-term form. This procedure is applied for both *host* matrix (pure PVP with τ_1^{host}, τ_2^{host}, τ_3^{host} lifetimes and I_1^{host}, I_2^{host}, I_3^{host} intensities) and NP-modified *guest-host* composite (As_4S_4-PVP with τ_1^*, τ_2^* , τ_3^* lifetimes and I_1^*, I_2^* , I_3^* intensities) like in Refs. [37,38]. The second component in this generalized x2-decomposition involves contributions from all possible trapping channels, including e^+ trapping, input from o-Ps decaying (formerly being in the third component with I_3^{host} or I_3^* intensities) and p-Ps self-decaying (formerly being in the first component with 0.125 ns lifetime and $1/3 \cdot I_3$ yield [16,17]). Thus, we can easily separate contributions to the first channel, which are different from p-Ps input, these being denoted as (τ_α,I_α) and (τ_α^*,I_α^*) for *host* and *host-guest* matrix, respectively. Under this condition, additional e^+ trapping input with lifetime τ_{int} and intensity I_{int} can be resolved in the second component of the generalized x2-term PAL spectrum of *host-guest* matrix (with remainder of o-Ps trapping sites taken as in *host* matrix) so that

$$I_2^* = I_{int} + I_3^* \cdot \left(I_2^{host} / I_3^{host} \right) \qquad (6)$$

$$\tau_2^* \cdot I_2^* = \tau_{int} \cdot I_{int} + \tau_2^{host} \cdot (I_2^* - I_{int}) \qquad (7)$$

The compensating (τ_n ,I_n) input in the first channel of NP- embedded composite arising from this additional e^+ trapping can be found under requirement of full equilibrium between channels:

$$\tau_n \cdot I_n / \tau_a^* \cdot I_a^* = \tau_{int} \cdot I_{int} / \tau_2^* \cdot I_2^*. \qquad (8)$$

Thereby, the physical parameterization of NP-related trapping sites can be finally performed by accepting (τ_n ,I_n) and (τ_{int}, I_{int}) as corresponding first and second components of x2-term PAL spectrum, where defect-related τ_{int} lifetime reflects e^+ trapping appeared due to embedded *guest* NP. Thus, by conversing experimental x3-term

PAL spectra of *host* PVP matrix and *host-quest* PVP - stabilized As_4S_4 nanocomposite in the generalized x2-term form in respect to *x3-x2-coupling decomposition* algorithm [36], we extract just this additive part which corresponds entirely to NP-related traps. Under accepted prerequisites, the e^+ trapping defects can be associated with pseudogap holes at the interface between outer surface layer of agglomerated *guest* NPs and innermost layer of surrounding *host* PVP matrix (as it was well outlined in Refs. [37,38]). The bulk positron lifetime τ_b calculated respectively to (τ_n ,I_n) and (τ_{int}, I_{int}) components using eq. (2) can be attributed to defect-free positron lifetime of distinct NP. In case of highly-monolith NPs, this τ_b value tends towards bulk positron lifetime of corresponding substance, while in more loose aggregates of many NPs, it is higher reflecting their inner compactness. In general, the value of tint lifetime itself, as well as its difference and ratio with bulk lifetime are attributed to geometrical size and nature of e^+ trapping interfacial holes, their trapping rate being estimated via two-state trapping formalism [16-18].

3. Results and discussion

3.1. Atomic-specific structure

The microstructure of PVP-stabilized tetra-arsenic tetra-sulfide As_4S_4 nanocomposites was studied with XRPD (Fig. 1). The XRPD pattern of reference pure PVP pellet (not shown in Fig. 1) testifies in a favor of its ideal amorphous state with two wide-stretched halos near 10.840 °2θ (the corresponding interplanar distance d = 8.155 Å) and 20.850 °2θ (d = 4.257 Å), in good agreement with known experimental data [39,40]. Thus, the revealed amorphous nature of PVP does not affect XRPD patterns of As_4S_4 crystalline phases allowing their reliable identification in nanocomposites.

The XRPD pattern of REA1 sample is shown in Fig. 1a. The high-temperature β-As_4S_4 phase prevails in this pellet giving in estimation 94.7 wt % in addition to arsenolite As_2O_3 phase of high crystallinity (5.3 wt %). The clearly observed decaying background and broad diffraction lines correspond to low crystallinity of this β-As_4S_4 phase (impact of amorphous phase is expected due to ball nanomilling). The refined unit-cell parameters and volume for the β-As_4S_4 phase (space group C2/c, a = 9.9395(11), b = 9.3649(10), c = 8.9028(11) Å, β = 102.224(7)° , V = 809.90(16) $Å^3$) are in good agreement with literature data, e.g. a = 9.958(2), b = 9.311(2), c = 8.867(2) Å, β = 102.57(1) , V = 802.43 $Å^3$ [41], but the unit-cell volume V is somewhat higher, indicated the possible influence of PVP-matrix. The estimated numerical value of average apparent crystallite size D for main peak reflexes of β-As_4S_4 approaches 35.1 nm, while average maximum strain ε achieves 0.01364. The XRPD pattern of initial non-milled sample, e.g. commercial arsenic(II) sulfide As_4S_4 supplied by Sigma-Aldrich, testifies in a favor of its better crystallinity. Nevertheless, the β-As_4S_4 phase is further dominant in this pellet with small addition of high-temperature dimorphite As_4S_3 phase. The estimated D value is higher (51.6 nm), in good respect to decreased strain in the powdered material (ε = 0.00953). Thus, despite evidently rough NPs morphology, the nanomilling does not change preferential crystalline state of this arsenical.

The XRPD pattern for REA2 sample milled from mineral realgar α-As_4S_4 is shown in Fig. 1b. This pattern also demonstrates low crystallinity and arsenolite As_2O_3 phase (6.6 wt %), which appears in addition to low-temperature α-As_4S_4 realgar phase (93.4 wt %). The refined unit-cell parameters and volume for α-As_4S_4 phase (space group $P2_1/n$, a = 9.3311(4), b = 13.5712(6), c = 6.5932(2) Å, β = 106.406(4)° , V = 800.93(6) $Å^3$) are in good agreement with literature data, e.g. a = 9.327(2), b = 13.563(1), c = 6.590(2) Å, β = 106.46(1)° , V = 799.48 $Å^3$ [42]. In contrast to REA1 sample, the latter gives an enlarged crystallite size D close to 63.4 nm with

ε = 0.00792. This α-As_4S_4r phase was also dominant in non-milled samples, giving D = 101.6 nm and ε = 0.00294.

The most complicated is chemical composition of sunlight exposured REA3 composites. As it follows from the XRPD pattern on Fig. 1c, this sample is also of low crystallinity with impurity arsenolite phase (6.0 wt %). This pellet is probably composed of a few As_4S_4 polymorphs, the most obvious of which can be ascribed to high-temperature β-As_4S_4 (~75 wt %) and pararealgar As_4S_4 (~19 wt %). Because of these crystallographically similar phases, it is difficult to calculate unambiguously crystallite size D and maximum microstrain ε in this nanocomposite (in respect to very rough estimation, the D = 32.5 nm is like in REA1 sample at obviously higher strain ε = 0.0155).

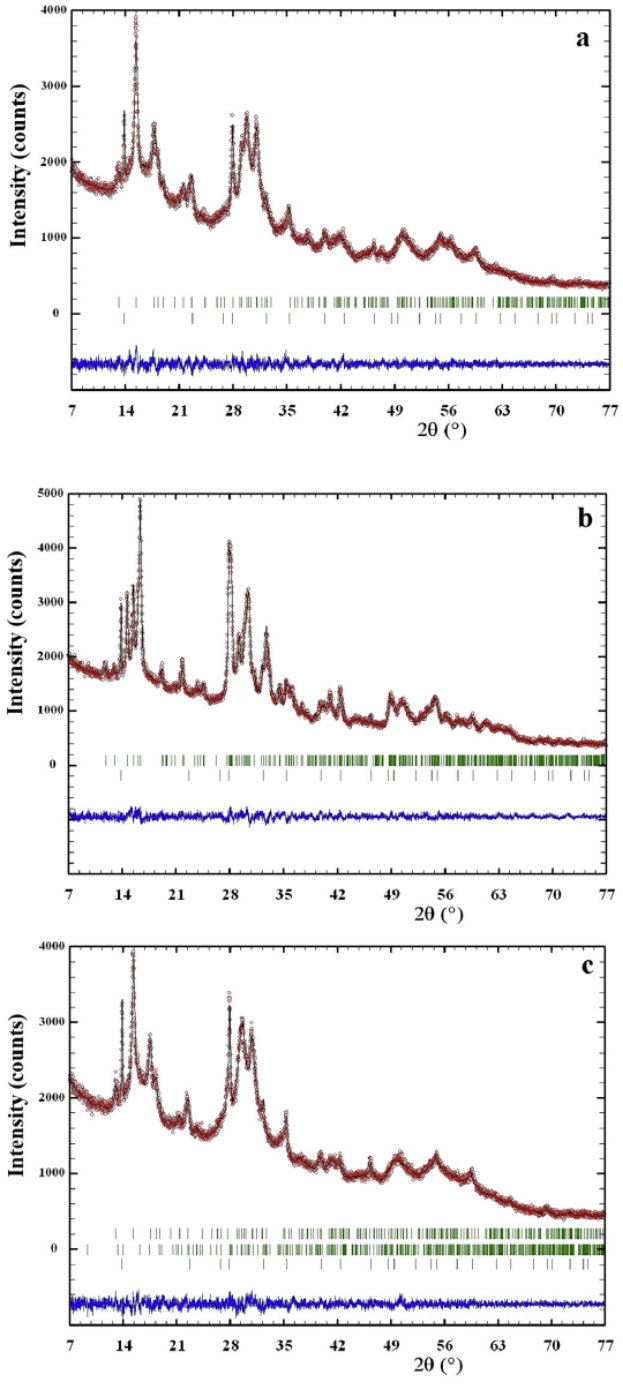

Fig. 1. Observed and calculated XRPD profiles for pelletized As_4S_4-PVP nanocomposites REA1 (a), REA2 (b) and REA3 (c): the experimental data (circles) and calculated profiles (solid line) are given with calculated Bragg positions (vertical ticks) for (a) β-As_4S_4 and arsenolite As_2O_3, (b) for a-realgar As_4S_4 and arsenolite As_2O_3 and (c) for a-realgar As_4S_4, pararealgar As_4S_4 and arsenolite As_2O_3 (the difference curves are given at the bottom by solid lines).

The results of XRPD analysis are agreed well with Raman scattering spectra collected in the region of 100-450 cm^{-1} as shown on Fig. 2. Since PVP does not contain any intrinsic vibrations in this region of interest [27,40], the main characteristic bands of Raman spectra are fully assigned to arsenical species, in full respect to known experimental data [28-34].

Preferential β-As_4S_4 phase of REA1 sample is identified from Raman-active modes revealed at background of wide-stretched fluorescent halo, these being 362, 343, 220 and 187 cm^{-1} (Fig. 2a). Because of this accompanied halo, the strict identification of other crystalline phases in this nanocomposite sample is difficult with Raman scattering technique.

In contrast, the α-As_4S_4 realgar phase is obviously dominant in REA2 sample based on mineral realgar as it follows from strong 184-194 cm^{-1} and weaker 167-173 cm^{-1} doublets, as well as intensive Raman scattering modes located near 370, 355 (the most intensive peak), 344, 222 and 145 cm^{-1} (Fig. 2b). The fluorescent halo is low and, correspondingly, the Raman scattering peaks of this phase are more clearly distinguished.

The high-temperature β-As_4S_4 phase is probably also present in REA3 pellet, but it being significantly superimposed by Raman-active modes originated from so-called χ-phase, which can be ascribed to intermediate precursor of pararealgar in light-induced alteration from α-As_4S_4 realgar (Fig. 2c). This polymorph was first introduced by Douglass et al. [43] as nucleating phase necessary to stabilize the reduced molecular symmetry of pararealgar with respect to realgar. This χ -phase is hardly identified from XRPD pattern since close proximity to structural fingerprints of pararealgar [29,30], but it exhibits clear Raman-active modes distinguishable from those proper to realgar and pararealgar As_4S_4. Thus, the peak centered near 186 cm^{-1} attains an abnormal growing, as well as Raman scattering in range of As-S stretching (300-400 cm^{-1} domain) clearly demonstrate strong separation for peaks at 344 cm^{-1} and 362 cm^{-1} (Fig. 2c). At the same time, the strong doublets at 230-236 cm^{-1} and 332-345 cm^{-1} proper to pararealgar [30] were not revealed in our spectra. Such configuration of Raman-active scattering modes was shown to be character for preference of χ-phase in a mixture with pararealgar taken in 2:1 ratio [30].

Identification of arsenolite As_2O_3 phase, which is present rather in small amount, is difficult because of overlapping corresponding Raman-active modes with those of arsenical polymorphs. Nevertheless, we detected an increase in shoulder near 80-85 cm^{-1} in Raman scattering spectra of all wet-milled samples as compared with initial non-milled ones, which could be treated in respect to [33,34] as direct signature of arsenolite As_2O_3. More reliable information on oxidation in nanomilled arsenicals can be extracted from SEM-EDS analysis.

The EDS spectra of typical ~25 μm^2 surface spots on REA1, REA2, REA3 pellets detected in narrow 0-3 keV domain are shown on Fig. 3a, b and 3c, respectively (the right-side presentation). As one can see from these figures, only arsenic As, sulphur S, oxygen O, carbon C and nitrogen N are main elements responsible for the peaks, located near ~1.28, 2.31, 0.53, 0.32 and 0.39 keV, respectively to Lα states of As, and Kα states of S, O, C and N. The high intensive As-lines in all EDS spectra correspond to As_4S_4 polymorphs despite difference in their crystalline forms. Strong C- and N-lines are obviously due to PVP environment, which is still essential in

these nanocomposites. But, the O-line is obviously enhanced as it could be expected from pure PVP environment, confirming extraoxidized state of nanomilled samples.

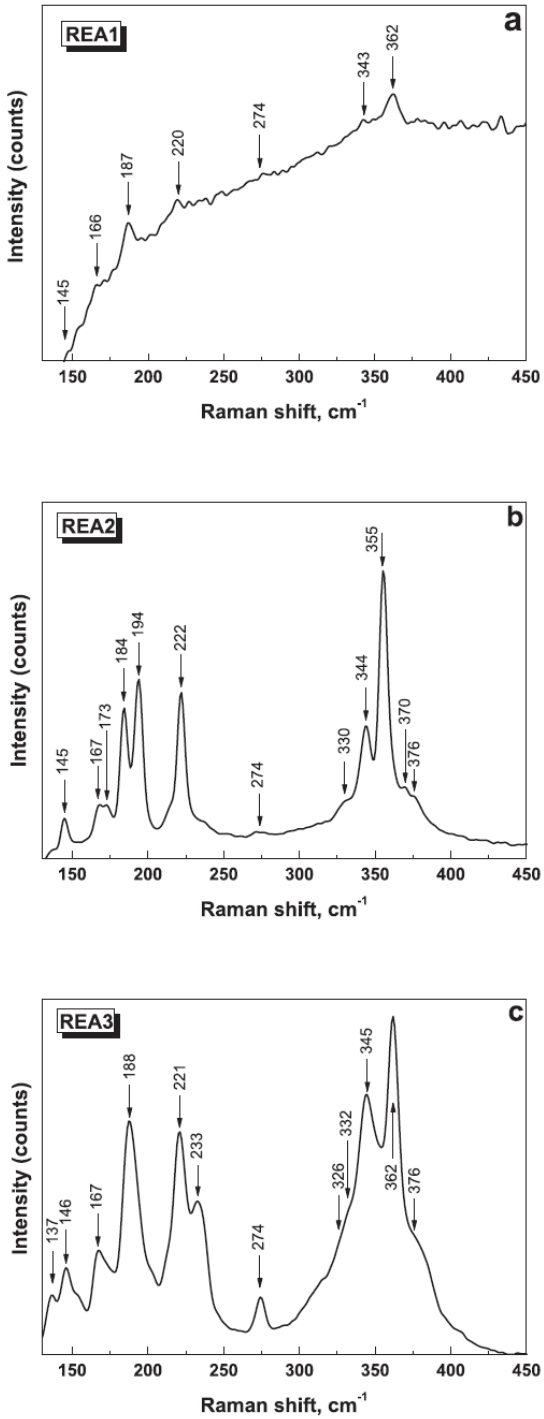

Fig. 2. Normalized Raman spectra collected from pelletized As_4S_4-PVP nanocomposites REA1 (a), REA2 (b) and REA3 (c).

The left-sided micrographs on Fig. 3 represent typical surface sections of As_4S_4-PVP pellets showing agglomerations of rhombohedral-shaped crystallites with character sizes of a few mm. Only visual inspection and comparison with similar surface extractions in light- [44-46] or high-energy irradiated As_2S_3 glasses [47,48] speak in a favor of their possible attribution to arsenolite As_2O_3 crystallites. Careful inspection along straight line crossing such crystals shows obvious increase in O-reflexes on the cost of S-ones without any essential

changes in As-related peak. So oxidation can be really activated by wet milling, this effect being revealed due to appearance of arsenolite As_2O_3 crystallites at the surface of As_4S_4-PVP nanocomposites. The reactive oxygen as a source for such chemical transformation can be employed from water solution of PVP, thus overall process can be distinguished as water-enhanced oxidation (the moisture acts as catalyst in As oxidation [44,45]). The initiating stage of such transformation is related to partial decomposition of arsenic sulfide, allowing demixing of elemental As for further direct interaction with O [44-48]. Therefore, one can speculate that decomposition of realgar polymorphs can be activated by wet milling resulting in final surface oxidation. For this reason, the nanomilled As_4S_4 is consequently recommended to subject the washing procedure such as described in Ref. [49], when it is aimed to be used for biological application (in order to eliminate surface contamination with As_2O_3).

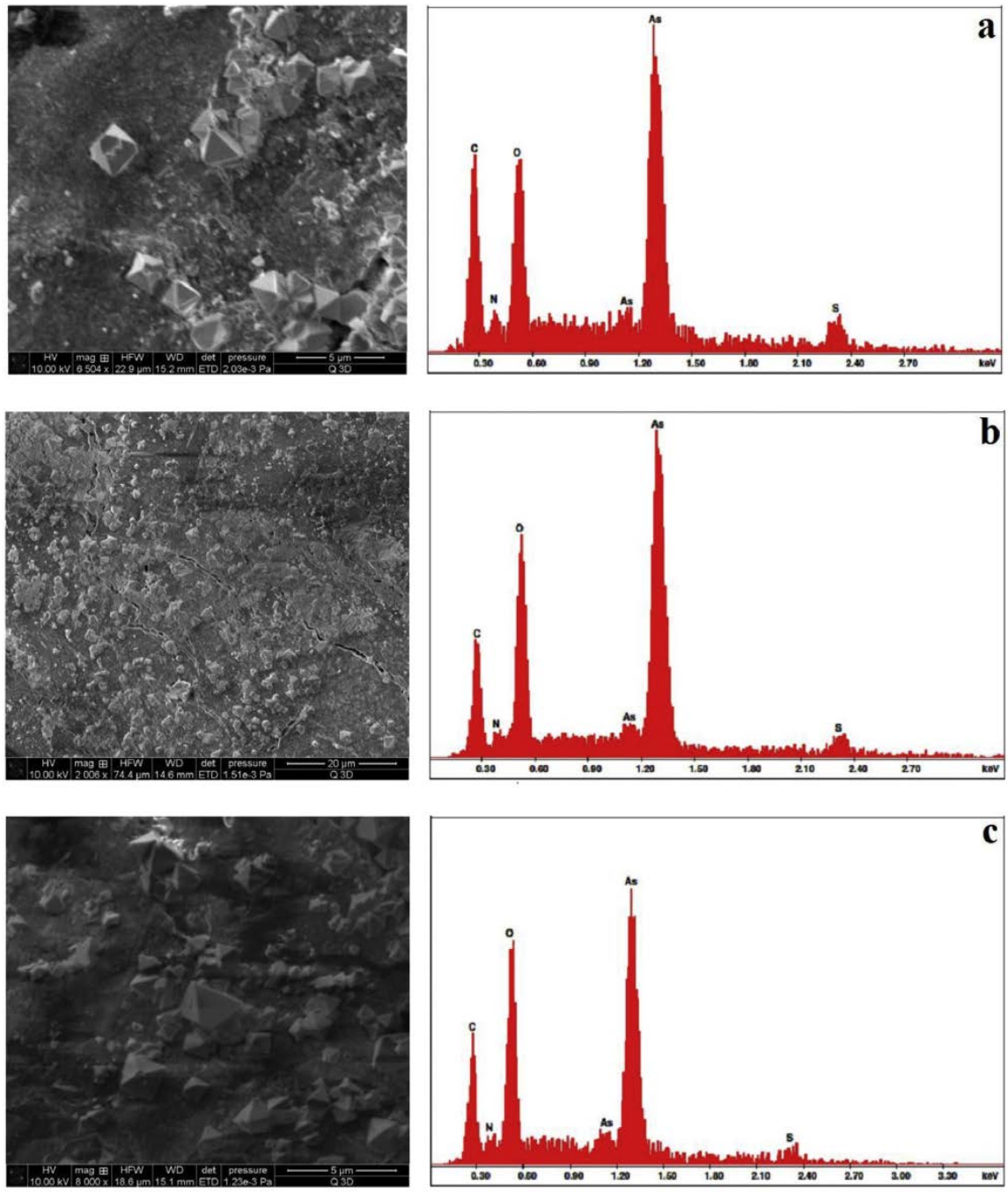

Fig. 3. SEM images showing extractions of arsenolite As_2O_3 crystals (left) and EDS spectrum detected from typical surface spots (right) of pelletized As_4S_4-PVP nanocomposites REA1 (a), REA2 (b) and REA3 (c).

3.2. Atomic-deficient structure

The raw PAL spectra of pure PVP and As_4S_4-PVP nanocomposites fitted in terms of minimal statistically weighted least-squares deviation between experimental points and theoretical curve built of three single exponents evolving inputs from both e^+ and Ps trapping channels are depicted in Fig. 4 (this spectrum is ascribed to REA1 pellet, other PAL spectra are not shown). Corresponding best fit e^+ and Ps trapping modes calculated within conventional approach considering non-separated inputs from these channels extracted from x3-decomposed PAL spectra are given in Table 1. The narrow values of statistical scatter of variance (MSD) tightly grouped around 0-axis testify that PAL measurements are adequately described by this fitting procedure.

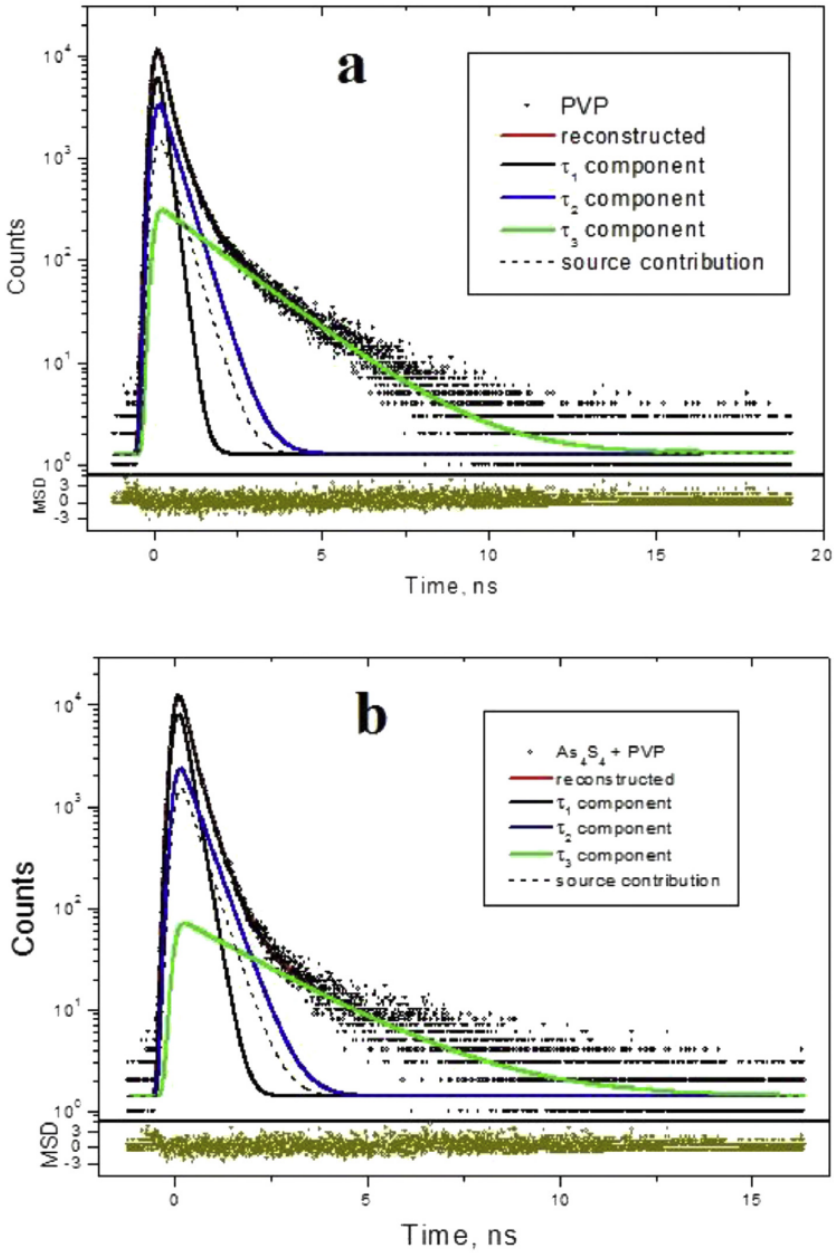

Fig. 4. Raw PAL spectra of (a) pure PVP and (b) pelletized As_4S_4-PVP nanocomposite REA1 reconstructed from x3-term fitting at the general background of source contribution (bottom insets show statistical scatter of variance).

In case of pure PVP pellet, the PAL spectrum (Fig. 4a) is characterized by long fluent decaying of coincidence counts in a time testifying in a favor of essential role of o-Ps trapping states [40].

Table 1
Fitting parameters and trapping modes determined within x3-decomposion procedure for experimental PAL spectra of pelletized As_4S_4-PVP nanocomposites [10].

Sample	Fitting parameters					e^+-trapping modes					R	f_v
	τ_1	τ_2	I_2	τ_3	I_3	$\tau_{av.}$	τ_b	κ_d	$\tau_2-\tau_b$	τ_2/τ_b		
	ns	ns	a.u.	ns	a.u.	ns	ns	ns^{-1}	ns	a.u.	nm	%
PVP	0.196	0.472	0.256	1.867	0.119	0.466	0.237	0.86	0.24	2.00	0.276	1.89
REA1	0.203	0.416	0.267	2.186	0.040	0.339	0.237	0.70	0.18	1.75	0.305	0.86
REA2	0.198	0.402	0.285	2.157	0.043	0.340	0.233	0.76	0.17	1.72	0.302	0.89
REA3	0.206	0.419	0.260	2.162	0.037	0.334	0.239	0.66	0.18	1.75	0.302	0.77

Formation of o-Ps is strongly inhibited by NPs in As_4S_4-PVP nanocomposites as it follows from lower intensity of the longest component due to drastic shortening in a tail of coincidence counts on Fig. 4b (the I_3 intensity reaches ~12% for pure PVP pellet and only ~4% for As_4S_4-PVP pellets). Correspondingly, the fractional free volume f_v recalculated in respect to eq. (5) with C constant taken as for epoxy-type polymers (C = 0.0018 [17]) decreases nearly twice going from pure PVP (f_v = 1.89%) to As_4S_4-PVP nanocomposites (f_v = 0.77-0.89%). At the same time, the mean radius of voids R defined from eq. (4) increases from 0.276 nm for PVP pellets (in respect to τ_3 = 1.867 ns) to ~0.30 nm for As_4S_4-PVP nanocomposites (in view of τ_3 deviation from 2.157 to 2.186 ns). This finding is in obvious contrast to [37], where decrease in R was observed for tiny spinel $NiFe_2O_4$ crystallites (a few nm) embedded in SiO_2 matrix. So effects of extra-small sizes are inessential in our case, whereas opposite growing trend due to coarse-grained As_4S_4 NPs in PVP matrix seems to be more plausible. This conclusion is well agreed with results of XRPD analysis, which confirm presence of rather rough As_4S_4 crystallites of 30-60 nm in sizes composing individual NP.

The same channel of o-Ps decaying is probably character for REA1, REA2 and REA3 pellets as it follows from results of conventional x3-decomposition procedure gathered in Table 1. Since neither τ_3, nor I_3 depend on the geometry of NP-forming crystallites, the channel of o-Ps decaying is presumably related to interfacial voids (holes) between respectively large NPs composed of smaller crystallites (30-60 nm). The observed changes in o-Ps decaying is accompanied by some changes in e^+ trapping states, revealed mainly in the second PAL component. Slight increase in I_2 intensity with more essential decrease in τ_2 lifetime is character for all As_4S_4-PVP pellets (in comparison with pure PVP pellets), provoking measurable decrease in eþ trapping rate (Table 1). The values of bulk defect-free lifetime τ_b calculated in respect to eq. (2) are only slightly changed as compared with pure PVP pellets, thus essentially complicating further analysis. Thereby, within conventional x3-term decomposition procedure, we can only declare some connection between eþ and Ps trapping channels caused by *guest* As_4S_4 NPs embedded in host PVP matrix.

To clarify the nature of NP-related void evolution in As_4S_4-PVP nanocomposites, the measured PAL data were treated within *x3-x2- coupling decomposition algorithm* [36], the results being presented in Table 2. Nearly the same $\tau_b \cong 0.24$ ns for all As_4S_4-PVP pellets determined within this algorithm for (τ_n, I_n) and (τ_{int}, I_{int}) as components of generalized x2-term decomposed PAL spectra, but which is evidently above bulk lifetime of 0.224 ns proper to realgar α-As_4S_4 crystal [50], testifies that e^+ trapping sites concern rather loosely-packed or efective As_4S_4 crystallites composing individual NP. The values of defect-related lifetimes of $t_{int} \cong$ 0.37-0.39 ns show that NP-related interfacial voids have character free volumes approaching ~80-100 $Å^3$ (near ~0.3 nm in radius in spherical approximation), as it follows from semi-empirical estimation for S-rich environment [18,51,52]. This conclusion agrees well with $(\tau_2 - \tau_b) \cong 0.15$ ns and $\tau_2/\tau_b \cong 1.6$ as characteristic fingerprints of triplet quadruple vacancies [16].

These findings are well reflected in atomic-deficient void structure of REA1 pellet, composed of high-temperature *β*-As_4S_4 polymorph (the source chemical arsenical taken from Sigma Aldrich, USA), owing to typical values of τ_{int} = 0.389 ns and τ_b = 0.240 ns. The most densified free-volume structure is character for REA2 pellet, composed of *α*-As_4S_4 polymorph (the mineral realgar taken as a source for milling). The lifetimes are minimal in this nanocomposite ($\tau_{int} \cong$ 0.368 ns and τ_b = 0.233 ns) because of smallest free volumes associated with agglomerated isocompositional NPs. If accept that both REA1 and REA2 nanocomposites are characterized by the same type of molecular building blocks (cage-like As_4S_4 molecules possessing D_{2d}

symmetry and ~14.8 $Å^3$ self-closed volume, composed by two As-As bonds in opposite orthogonal configurations interlinked via four As-S-As bridges [49,53,54]), this enhanced atomic compactness can be probably accepted as responsible for better anticancer activity of REA2 suspension [10]. Thus, the IC_{50} parameter (which is 50% concentration of arsenical corresponding to the inhibition effect) on H460 human lung cell is twice reduced with transition from REA1 (0.066 mg/mL) to REA2 suspension (0.033 mg/mL) [10], thus reflecting positive impact of local As concentration on this cancer cell.

The largest values of τ_{int} = 0.396 ns and τ_b = 0.244 ns are proper to REA3 pellet having most complicated phase composition (~75 wt % of β-As_4S_4 and ~19 wt % of pararealgar As_4S_4 with intermediate χ -phase, in respect to XRPD and Raman scattering analysis). This nanocomposite is built of loosely packed NPs with largest e^+ trapping free-volume voids. Nevertheless, corresponding nanosuspension demonstrates well-expressed anticancer activity in respect to IC_{50} = 0.031 μg/mL [10], which evidently follows from its chemistry enriched on pararealgar As_4S_4 phase. Positive effect of densified local As environment in this case is realized due to specificity of pararealgar molecules of C_s symmetry and nearly ~15.7 $Å^3$ self-closed volume, having three As atoms forming two adjacent homonuclear As-As bonds in heteronuclear As-S neighboring [54,55]. Comparing e^+ trapping modes gathered in Table 2 for this REA3 sample with REA2 one (where α-As_4S_4 realgar phase is dominant), we conclude that most perfect structure of As_4S_4 polymorphs composing NPs corresponds to smallest free volumes associated with them.

Table 2
NP-related PAL trapping modes in pelletized As_4S_4-PVP nanocomposites treated within x3-x2-coupling decomposition algorithm.

Sample (in respect to pure PVP)	First component		Second component		e^+-trapping modes				
	τ_n	I_n	τ_{int}	I_{int}	τ_{av}	τ_b	κ_d	$\tau_2-\tau_b$	τ_2/τ_b
	ns	a.u.	ns	a.u.	ns	ns	ns^{-1}	ns	a.u.
REA1	0.207	0.427	0.389	0.181	0.261	0.240	0.68	0.15	1.62
REA2	0.199	0.409	0.368	0.199	0.253	0.233	0.74	0.14	1.58
REA3	0.211	0.445	0.396	0.180	0.264	0.244	0.64	0.15	1.62

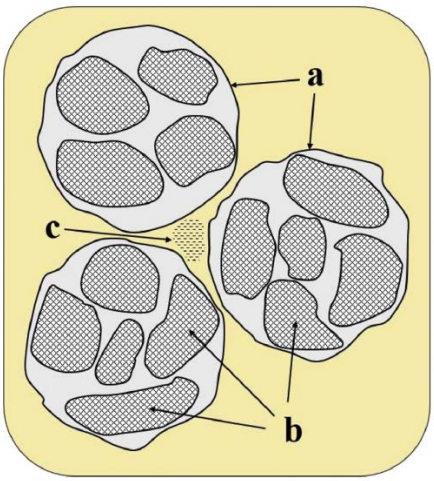

Fig. 5. Schematic illustration of microstructure fragment depicting expected PAL channels in As_4S_4-PVP nanocomposites: individual NPs (a) composed of distinct As_4S_4 crystallites (b), forming interfacial e^+ -trapping holes (c).

So at the basis of these findings, the microstructure model of mixed e^+-Ps trapping in As_4S_4-PVP nanocomposites can be validated as shown in Fig. 5. The REA1, REA2 and REA3 pellets are composed of individual NPs of relatively large size (nearly above hundred of nm like as in freshly-prepared suspensions [10]), which are more or less uniformly embedded in PVP environment. Since these sizes are smaller than typical e^+

diffusion lengths (no more than a few tens of nm in semiconductors [16,17]), the positrons thermalized within individual NPs will contribute to annihilation outside them tending the overall trapping process towards saturation. Thus, the NP-related e^+ trapping occurs preferentially in PVP medium of interfacial holes created by neighboring NPs. The NPs are loosely composed from a few As_4S_4 crystallites, these being in respect to main crystallographic polymorphs used for high-energy milling. It is noteworthy that oxidation provoked by wet milling does not influence above conclusions. This is because of presumably the same impact of oxidation in all pellets (the content of admixed As_2O_3 phase is close to 6 wt %), as well as preference of volumetric e^+-Ps trapping sites inside sample's bulk over surface related traps.

4. Conclusions

Nanostructurization in PVP-stabilized nanocomposites of tetra-arsenic tetra-sulfide As_4S_4 polymorphs was studied with complementary atomic-specific (XRPD, Raman scattering and SEM with EDS analysis) and atomic-deficient (PAL spectroscopy) characterization probes allowing reliable identification of all products formed under wet milling. It was shown that phase compositions of the pelletized nanocomposites were in strong relation to coarse counterparts used for milling with surface extraction of arsenolite As_2O_3 crystallites. The PAL data treated in terms of substitution e^+-Ps trapping were adequately used to describe transformation of o-Ps trapping sites in pure PVP matrix into e^+ trapping sites in NP-modified matrix. The modified x3-x2-coupling decomposition algorithm developed in addition to conventional x3-term decomposition route was applied to parameterize expected annihilation channels in these inhomogeneous solids. Interfacial free-volume voids created by neighboring NPs embedded in PVP environment were defined as most efficient e^+ trapping sites. Within developed model, the NPs themselves were imagined as loosely composed by few As_4S_4 crystallites proper to main polymorphs used for milling.

Acknowledgements

This work was supported by Slovak Research and Development Agency (contract No. APVV-14-0103) and bilateral project SK-UA-2013-0003. ShYa is grateful to SAIA (contract No. 17753) for financial support within National Scholarship Program of the Slovak Republic.

References

[1] P.J. Dilda, P.J. Hogg, Arsenical-based cancer drugs, Cancer Treat. Rev. 33 (2007) 542-564.

[2] J. Liu, Y. Lu, Q. Wu, R.A. Goyer, M.P. Waalkes, Mineral arsenicals in traditional medicines: orpiment, realgar, and arsenolite, J. Pharmacol. Exp. Ther. 326 (2008) 363-368.

[3] S. Gibaut, G. Jaouen, Arsenic-based drugs: from Fowler's solution to modern anticancer chemotherapy, Top. Organomet. Chem. 32 (2010) 1-20.

[4] Z.-Y. Wang, Arsenic compounds as anticancer agents, Cancer Chemother. Pharmacol. 48 (2001) S72-S76.

[5] Y. Tian, X. Wang, R. Xi, W. Pan, S. Jiang, Z. Li, Y. Zhao, G. Gao, D. Liu, Enhanced antitumor activity of realgar mediated by milling it to nanosize, Intern. J. Nanomed. 9 (2014) 745-757.

[6] Y. Deng, H. Xu, K. Huang, X. Yang, C. Xie, J. Wu, Size effects of realgar particles on apoptosis in a human umbilical vein endothelial cell line: ECV-304, Pharmacol. Res. 44 (2001) 513-518.

[7] J.-Z. Wu, P.C. Ho, Evaluation of the in vitro activity and in vivo bioavailability of realgar nanoparticles prepared by cryogrinding, Eur. J. Pharm. Sci. 29 (2006) 35-44.

[8] P. Bala , W.S. Choi, E. Dutkov , Mechanochemical modification of properties a and reactivity of nanosized arsenic sulphide As4S4, J. Phys. Chem. Solids 68 (2007) 1178-1183.

[9] M. Lin, Z. Wang, D. Zhang, Cytotoxic effect of As2S3 nanoparticles on liver cancer cells, in: Proc. of the 1st IEEE Intern. Conf. on Nano/micro Engineered and Molecular Systems. Jan. 18-21, 2006. Zhuhai, China, 2006, pp. 923-927.

[10] Z. Bujnakova, P. Balaz, P. Makreski, G. Jovanovski, M. Caplovicova, L. Caplovic, O. Shpotyuk, A. Ingram, T.-C. Lee, J.-J. Cheng, J. Sedlak, E. Turianicova, A. Zorkovska, Arsenic sulfide nanoparticles prepared by milling: properties, free-volume characterization, and anti-cancer effects, J. Mater. Sci. 50 (2015) 1973-1985.

[11] M. Pastorek, P. Gronesova, L. Cholujova, Z. Bujnakova, P. Bal , J. Duraj, T.C. Lee, J. Sedlak, Realgar (As_4S_4) nanoparticles and arsenic trioxide (As_2O_3) induced autophagy and apoptosis in human melanoma cells in vitro, Neoplasma 61 (2014) 700-709.

[12] N. Wang, L.-W. Wang, B.-D. Gou, T.-L. Zhang, Preparation of realgar nanoparticle suspension and its inhibition effect on the proliferation of human myelocytic leukaemia HL-60 cells, J. Dispecsion Sci. Technol. 30 (2009) 237-240.

[13] S.-J. Ou, X.-C. Shen, T. Jin, J. Xie, Y.-F. Cuo, H. Liang, R.-B. Hou, Polymer-directed assembly of water-soluble realgar nanocomposites for antimicrobial applications, Front. Mater. Sci. China 4 (2010) 339-344.

[14] R. Cheng, M. Zhang, Preparation, characterization and antimicrobial activities of polymer/realgar nanocomposites, J. Exper. Nanosci. 8 (2013) 61-68.

[15] A.C. Balazs, T. Emrick, T.P. Russell, Nanoparticle polymer composites: where two small worlds meet, Science 314 (2006) 1107-1110.

[16] R. Krause-Rehberg, H. Leipner, Positron Annihilation in Semiconductors: Defect Studies, Springer, Heidelberg, 1999.

[17] Y.C. Jean, P.E. Mallon, D.M. Schrader, Principles and Application of Positron and Positronium Chemistry, World Sci. Publ. Co. Pte. Ltd., New Jersy-London- Singapore-Hong Kong, 2003.

[18] O. Shpotyuk, J. Filipecki, Free Volume in Vitreous Chalcogenide Semiconductors: Possibilities of Positron Annihilation Lifetime Study, 2003. Ed. WSP, Czestochowa.

[19] Stoe WinXPOW (Version 3.03), Stoe & Cie GmbH, Darmstadt, Germany, 2010.

[20] W. Kraus, G. Nolze, POWDER CELL - a program for the representation and manipulation of crystal structures and calculation of the resulting X-ray powder patterns, J. Appl. Cryst. 29 (1996) 301-303.

[21] R.T. Downs, M. Hall-Wallace, The American mineralogist crystal structure database, Am. Mineral. 88 (2003) 247-250. http://rruff.geo.arizona.edu/AMS/amcsd.php.

[22] P. Villars, K. Cenzual (Eds.), Pearson's Crystal Data: Crystal Structure Database for Inorganic Compounds, Release 2013/14, ASM International, Materials Park, OH, 2013.

[23] J. Rodriguez-Carvajal, Recent developments of the program FullProf. Commission on powder diffraction (IUCr), Newsletter 26 (2001) 12-19.

[24] R.J. Hill, C.J. Howard, Quantitative phase analysis from neutron powder diffraction data using the Rietveld method, J. Appl. Crystallogr. 20 (1987) 467-474.

[25] J. Rodriguez-Carvajal, T. Roisnel, Line broadening analysis using FullProf: determination of microstructural properties, Mater. Sci. Forum 443-444 (2004) 123-126.

[26] R. Golovchak, O. Shpotyuk, A. Kozdras, M. Vlcek, B. Bureau, A. Kovalskiy, H. Jain, Long-term physical ageing in AseSe glasses with short chalcogen chains, J. Phys. Condens. Matter 20 (2008), 245101-1-245101-7.

[27] Y. Borodko, S.E. Habas, M. Koebel, P. Yang, H. Frei, G.A. Somorjai, Probing the interaction of poly(vinylpyrrolidone) with platinum nanocrystals by UV-Raman and FTIR, J. Phys. Chem. B 110 (2006) 23052-23059.

[28] W. Bues, M. Somer, W. Brockner, Schwingungsspektren von As_4S_4 und As_4Se_4, Z. Anor. Allg. Chem. 499 (1983) 7-14.

[29] P. Bonazzi, S. Manchetti, G. Pratesi, M. Muniz-Miranda, G. Sbrana, Light-induced variations in realgar and b-As4S4: X-ray diffraction and Raman studies, Am. Mineral. 81 (1996) 874-880.

[30] K. Trentelman, L. Stodulski, Characterization of pararealgar and other light-induced transformation products from realgar by Raman microspectroscopy, Anal. Chem. 68 (1996) 1755-1761.

[31] D.G. Georgiev, P. Boolchand, K.A. Jackson, Intrinsic nanoscale phase separation of bulk As_2S_3 glass, Philos. Mag. 83 (2003) 2941-2953.

[32] P. Chen, C. Holbrook, P. Boolchand, D.G. Georgiev, K.A. Jackson, M. Micoulaut, Intermediate phase, network demixing, bosob and floppy modes, and compositional trends in glass transition temperatures of binary As_xS_{1-x} system, Phys. Rev. B 78 (2008), 224208-1224208-15.

[33] S.J. Gilliam, C.N. Merrow, S.J. Kirkby, J.O. Jensen, D. Zeroka, A. Banerjee, Raman spectroscopy of arsenolite: crystalline cubic As4O6, J. Solid State Chem. 173 (2003) 54-58.

[34] A. Grzechnik, Compressibility and vibrational modes in solid As_4O_6, J. Solid State Chem. 144 (1999) 416-422.

[35] J. Kansy, Microcomputer program for analysis of positron annihilation lifetime spectra, Nucl. Instr. Meth. Phys. Res. A 374 (1996) 235-244.

[36] O. Shpotyuk, J. Filipecki, A. Ingram, R. Golovchak, M. Vakiv, H. Klym, V. Balitska, M. Shpotyuk, A. Kozdras, Positronics of subnanometer atomistic imperfections in solids as a high-informative structure characterization tool, Nanoscale Res. Lett. 10 (2015), 77-1-77-5.

[37] S. Chakraverty, S. Mitra, K. Mandal, P.M.G. Nambissan, S. Chattopadhyay, Positron annihilation studies of some anomalous features of $NiFe_2O_4$ nanocrystals grown in SiO_2, Phys. Rev. B 71 (2005), 024115-1-024115-8.

[38] S. Mitra, K. Mandal, S. Sinha, P.M.G. Nambissan, S. Kumar, Size and temperature dependent cationic redistribution in $NiFe_2O_4$ (SiO_2) nanocomposites: positron annihilation and Mossbauer studies, J. Phys. D. Appl. Phys. 39 (2006) 4228-4235.

[39] K. Sivaiach, K.N. Kumar, S. Buddhudu, Structural and optical properties of Liþ: PVP & Ag+: PVP polymer films, Mat. Sci. Appl. 2 (2011) 1688e1696.

[40] O. Shpotyuk, Z. Bujnakova , P. Balaz, A. Ingram, Y. Shpotyuk, Positron annihilation lifetime study of polyvinylpyrrolidone for nanoparticle-stabilizing pharmaceuticals, J. Pharm. Biomed. Anal. 117 (2016) 419-425.

[41] P. Bonazzi, L. Bindi, G. Pratesi, S. Menchetti, Light-induced changes in molecular arsenic sulfides: state of the art and new evidence by single-crystal X-ray diffraction, Am. Mineral. 91 (2006) 1323-1330.

[42] A. Kyono, M. Kimata, T. Hatta, Light-induced degradation dynamics in realgar: in situ structural investigation using single-crystal X-ray diffraction study and X-ray photoelectron spectroscopy, Am. Mineral. 90 (2005) 1563-1570.

[43] D.L. Douglass, C. Shing, G. Wang, The light-induced alteration of realgar to pararealgar, Am. Mineral. 77 (1992) 1266-1274.

[44] J.S. Berkes, S.W. Ing Jr., W.J. Hillegas, Photodecomposition of amorphous As_2Se_3 and As_2S_3, J. Appl. Phys. 42 (1971) 4908-4916.

[45] S.A. Keneman, J. Borgoda, J.N. Zemel, Evaporated films of arsenic trisulfide: physical model of effects of light exposure and heat cycling, J. Appl. Phys. 49 (1978) 4663-4673.

[46] P.J. Allen, B.R. Johnson, B.J. Riley, Photo-oxidation of thermally evaporated As_2S_3 thin films, J. Optoelectron. Adv. Mater. 7 (2005) 1759-1764.

[47] O.I. Shpotyuk, Semiconducting chalcogenide glass 1: glass formation, structure, and simulated transformations in chalcogenide glassess, in: R. Fairman, B. Ushkov (Eds.), Semiconductors and Semimetals, vol. 78, Elsevier Academic Press, 2004. Amsterdam-Boston-London-New York-Oxford-Paris-San Diego-San Francisco-Singapore-Sydney-Tokyo.

[48] M. Shpotyuk, O. Shpotyuk, R. Serkiz, P. Demchenko, S. Kozyukhin, Surface oxidation in glassy arsenic trisulphide induced by high-energy γ-irradiation, Rad. Phys. Chem. 97 (2014) 341-345.

[49] P. Balaz , A.V. Nguyen, M. Fabian, D. Cholujova, M. Pastorek, J. Sedlak, Z. Bujnakova, Properties of arsenic sulphide As_4S_4 nanoparticles prepared by high-energy milling, Powder Technol. 211 (2011) 232-236.

[50] O. Shpotyuk, A. Ingram, P. Demchenko, Free volume structure of realgar α-As_4S_4 by positron annihilation lifetime spectroscopy, J. Phys. Chem. Sol. 79 (2015) 49-54.

[51] O. Shpotyuk, A. Ingram, M. Shpotyuk, J. Filipecki, Prediction of free-volume-type correlations in glassy chalcogenides from positron lifetime measurements, Nucl. Instr. Meth. Phys. Res. B 338 (2014) 66-71.

[52] O. Shpotyuk, J. Filipecki, M. Shpotyuk, A. Ingram, Free volume evolution in chalcogenide glasses as probed by PAL spectroscopy, Solid State Ionics 267 (2014) 38-43.

[53] T. Ito, N. Morimoto, R. Sadanaga, The crystal structure of realgar, Acta Cryst. 5 (1952) 775-782.

[54] P. Bonazzi, L. Bindi, A crystallographic review of arsenic sulfides: effects of chemical variations and changes induced by exposure to light, Z. Ktistallogr. 223 (2008) 132-147.

[55] P. Bonazzi, S. Menchetti, G. Pratesi, The crystal structure of pararealgar, As_4S_4, Am. Mineral. 80 (1995) 400-403.